Particle trajectories around solid or fluid obstacle in microfluidic channels

by

Tianyu Yan

A thesis submitted to Johns Hopkins University in conformity with the requirements for the degree of Master of Science in Engineering

Baltimore, Maryland

July 2016

Abstract

Particle separation is a technological area where microfluidics shows promises towards miniaturization, specificity, and throughput. We study here the mechanisms for particle separation in deterministic lateral displacement (DLD), a size-based microfluidic particle separation method. The experiments are also designed to be a model system for colloidal transport on solid-water (SWI) and air-water (AWI) in subsurface. To mimic particle transport around the obstacles in DLD we developed a simple but versatile microfluidic platform in which the particles' trajectories are tracked during their motion around an individual solid (PDMS) or fluid (bubble) obstacle.

The trajectories of individual particles passing an obstacle are analyzed using a collision model[1]. In this model there are two types of particle–obstacle collisions. The hydrodynamic collisions are reversible with symmetric trajectories around the obstacle. The touching collisions are irreversible with asymmetric trajectories. We characterize the type of collision for particles transport via both pressure-driven flow and gravity-driven transport. Only hydrodynamic collisions are observed with pressure-driven flow as the particles follow symmetric trajectories with respect to the obstacle. We also do not observe adsorption of the particles to either the AWI or SWI. In contrast, we observe both symmetric and asymmetric particle trajectories for gravity-driven particle transport. We observe a transition from symmetric to asymmetric trajectories as the impact point between the particle and the obstacle moves from the top to closer to the center of the obstacle. We find that the transition between symmetric and asymmetric

trajectories depends on the particle size and show that we can rely on this size dependence for particle separation. In addition, we find that particles around fluid obstacle have smaller transitioning impact point than that of solid obstacle even if the obstacles have nearly same size and shape.

Advisor: Dr. Joëlle Fréchette

Reader: Dr. German Drazer

Acknowledgement

Here I want to take this opportunity to express my gratitude to all the people who helped me in the past two years. First, I would like to show my appreciation to my advisor Dr. Joëlle Fréchette and our collaborator Dr. German Drazer. They shared their creativity with me, gave me priceless guidance in my progress and lead my research ability to a higher level.

I also want to say thanks to Dr. Zachary Gagnon, Dr. Michael. Bevan and their lab members, who provided me technically support in my project.

I feel privileged to have had teammates like Yumo, Charles, Xiaoqing, Leo, Georgia, Xue, Preetika, Nikki, Chris and Robert. Without their help, this project wouldn't be done successfully. Their kindness supported me to go through these days no matter how tough the research was.

I would like to say thanks to my friends: Xiaotong, Xinpei, Yang, Hao, Liangyu and Bin. Without their encouragement and help, I couldn't adhere to this path and come so far.

At last I really appreciate all the supports from my parents and family. They backed up my life and stay with me no matter what I was facing to. Their loves make up the best part of my life.

Table of Contents

List of Figures

List of Tables

Chapter 1. Introduction

1.1 Importance of hydrodynamic-based separation methods in microfluidic devices

Hydrodynamic separation is a type of technology that utilize the hydrodynamic interactions between geometries in microfluidic devices and the species being sorted, which is widely involved in medical tests, biochemical essays, chemical processing and environmental assessment. One advantage of microfluidic separation technique is the small sample volume required, which results in less cost of reagents and device fabrication, continuous operation, shorter analysis period and minimal invasive during sample extraction from patients or experimental animals.

As a representative of hydrodynamic separation, deterministic lateral displacement (DLD) relies on how the trajectory of particle is affected by the presence of a nearby obstacle[2] (as shown in Fig. 1). The mechanisms for hydrodynamic separation has been the subject of various studies, due to its importance in biochemical assays[3], cell manipulation[4], environmental test[5]. Its profound impact and numerous applications have aroused scientists' interests in the past decade. For example, the tendency of the self-propelled particles (SPPs) to attach to solid surfaces has been reported[6]. Tissue-like multilayer cellular structures (MLCs) have been utilized to investigate gold nanoparticles(GNPs) interaction at interfaces in nano/ micron scale[7]. In pinched flow fractionation[8], particles entering a constriction and exiting into a sudden expansion experience a lateral displacement and separated by the spreading streamlines according

to their sizes. Deterministic lateral displacement (DLD)[9] makes use of asymmetric

bifurcation of laminar flow around a periodic array of solid obstacles, thus particles

deterministically select their path base on their size and deformability.
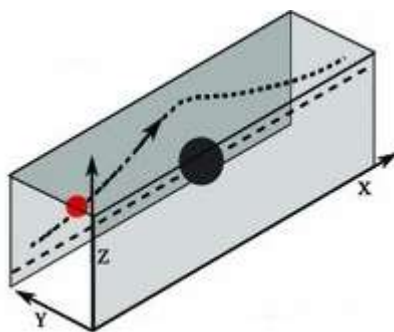
Figure 1. *An example of particle pass the constriction created by a plane wall and spherical obstacle[2]. Adapted from Risbud, S et al. (2014)*

1.2 Overview of microfluidic Products

With the growing interest in device miniaturization, microfluidics, which is also

known as Lab-on-Chip (LOC), products are widely used in various fields of research.

The fast reaction times, small sample volume required, and avoidance of cross-

contamination make LOC products ideal platforms for analytical chemistry, biological

analysis, and medical tests.

The silicon-based (e.g. glass and quartz) microfluidic device first came out due to the

development of silicon fabrication technology in 1980s[10]. Nevertheless, the silicon-

based microdevices also have weaknesses namely, expensive, fragile and complicated

to fabricate or duplicate. Driven by these shortcomings, scientists tend to find superior

substitutes in terms of simplified fabrication process, reduced costs, and increasing

robustness. Consequently, various polymer-based plastic materials, such as

poly(dimethylsiloxane) (PDMS)[11, 12], poly(methylmethacrylate) (PMMA)[12, 13], polycarbonate (PC)[14, 15], polyimide (PI)[16, 17], and poly(ethylene terephthalate) (PET) [18] have dominated in microfluidic products through the past few decades. One of the most commonly used polymer is a transparent silicone elastomer, polydimethylsiloxane (PDMS). It has been most widely applied in micro-fabrication due to a simple and versatile molding process, biocompatibility, low-cost, high thermal resistance, optical transparency in visible wavelengths[19]. Bonding is one of the key steps in micro-fabrication. Strong device assembly can be achieved by introducing surface hydroxyl groups via plasma treatment[13] followed by thermal curing[20]. In general, PDMS, together with silicon wafer and glass, make up a fundamental microfluidic platform.

Since the dimensions of microfluidic products have reached micron scale, some traditional limits on biological process or chemical reactions are eliminated to some extent, for heat transfer, diffusion rate and reaction rate could rise dramatically.[21] This nature enables microfluidic technology with small sample consumption, high sensitivity, and fast response time.[22] For these benefits, practical microfluidic technologies have been widely applied in various fields such as biochemical assays[3], cell manipulation[4], environmental test[5], etc.

Advantages	Disadvantages
Increased spatial resolution	Low signal-to-noise ratio
Automated measurement	Insufficient precision and accuracy
Robustness	Unknown physical and chemical effects
User-friendly interfaces	Not yet integrated with novel technology
Portability and disposability	
New opportunities for integrated chips	

Table 1. *Advantages and disadvantages of LOC products[23].*

1.3 Applications of hydrodynamic interactions between particles and obstacles

The nature of hydrodynamic separation in microfluidic devices is particle behaviors near obstacle with restriction[2]. This also provides simple model to mimic numerous phenomenon in micro- or macroscale, including emulsions, flotation, and transport in porous media, which will be discussed in the following paragraphs.

1.3.1 Transport of particles in porous media

Micro-models have been utilized as valuable tools to investigate and visualize the transport of particulates in unsaturated porous media. They have been employed in various areas, such as displacement mechanisms for water/ air or oil in porous media[24, 25](as shown in Fig. 2), multiphase fluid distribution and flow at permeability boundaries[26], role of surface chemistry in colloidal interfacial retention at the pore

scale[27], energy issues in multiphase transport within porous media[28], reservoir on- a-chip[29].

To visualize particles' behavior using the micromodel, an open-end micro-channel and microscopy are indispensable. Initially, visualization of colloids dynamics within unsaturated media were performed in glass micro-models under optical fluorescent microscopy, where the air phase was static with steady aqueous phase flow[30, 31]. Later, air bubbles were injected into etched glass micro-channels so as to study colloids interaction with a single air bubble at pore scale[32, 33]. Since 1980s, silicon-based micro-chips have been used to study colloids behaviors in porous medium[34]. Compared to glass and silicon, a soft material like PDMS[11, 12] or PMMA[12, 13] is preferred since these elastomers are less expensive or fragile and easier to fabricate or duplicate.

The colloidal attachment and mobilization in presence of fluid/fluids or fluids/solid interfaces within unsaturated porous media has been widely investigated. Optical microscopy generates an overall image of the whole channel depth, while confocal microscope, could focus and obtain images of colloids-fluid interaction at various depths within the channel. Fluorescent dyed fluids or fluorescent particles is necessary in confocal microscopy. In this way, the sample can be imaged spatially in 3D by superposing two dimensional images taken at sequential z stacks[35].
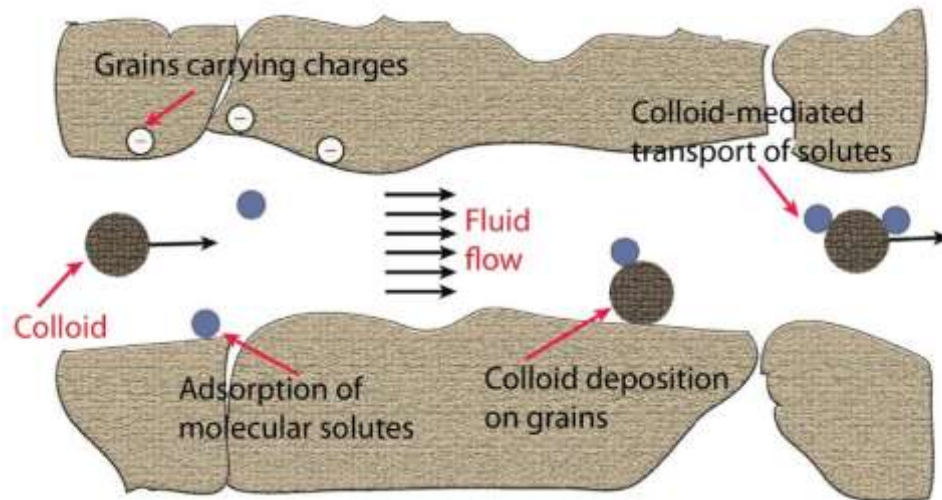
Figure 2. Flow and transport of colloidal particles attached with possible radioactive contaminants[36]. Adapted from Sharma, P et al. (2012).

1.3.2 Flotation

Flotation is a physicochemical process that makes use of the difference in the surface properties of the wanted and unwanted particles. It is a common separation method in various industries, e.g. mining[37], waste water treatment[38] and paper recycling[39]. It involves interaction between solid, liquid and air phases, which is manipulated by the bubble–particle attachment mechanism. Scientists have studied bubble–particle attachment mechanism in numerous aspects, such as bubble–particle attachment time[40], particle dropping technique[41], AFM bubble–particle measurements[42, 43], bubble and particle zeta potential measurements[44], and flotation recovery experiments[45, 46].

During flotation, particles and bubbles collide, and hydrophobic particles might get attached by bubbles[47-49], as shown in Fig. 3. These particle-bubble attachment were collected by selective reagents, transported to the froth zone whereas the hydrophilic particles remain in the liquid phase. Surface chemistry of both particles and air bubbles

affect the bubble–particle attachment[47-49]. For example, surface chemistry of particles

could be controlled by reagents adsorption onto particle surfaces, which makes particles

more hydrophobic.

Induction time, t_{ind}, is a key parameter characterizing the probability of particle–

bubble attachment, which was first identified by Sven-Nilsson in 1934. In flotation the

induction time can be interpreted as a threshold sliding duration[48]. On particle is

approaching bubble, it will first deviate from its initial trajectory, due to the fluid forces,

and then it will slide over the bubble's surface for a while, t_{slide}. If $t_{slide} < t_{ind}$, then

attachment is unlikely to happen; conversely if $t_{slide} > t_{ind}$, then attachment is expected to

happen.
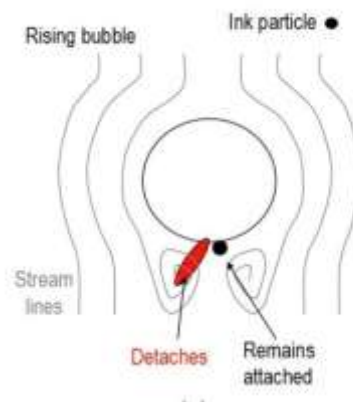
Figure 3. *Scheme of particle attachment and flotation during the flotation deinking process[50].*
Adapted from Beneventi, D. et al. (2010).

1.3.3 Pickering Emulsion

Named after S.U. Pickering[51], Pickering emulsions are stabilized by solid particles,

which adsorb onto the interface between the two phases(usually oil/water), as shown in

Fig. 4. They are widely used in food industry[52], life sciences[53] and materials science[54].

While lots of emulsions are stabilized by surfactants, the mechanism of solid particle adsorption is different from surfactants, because the particles do not have to be amphiphilic. The substitution of solid particles makes the Pickering emulsion highly stable against coalescence. In addition, the Pickering emulsions are preferred in areas where surfactants often bring about side effects, especially in cosmetic and pharmaceutical products. Solid stabilizing particles are usually smaller than emulsion droplets. Unlike classical emulsions, the utilization of solid particles in micrometer, results in stabilization of droplets and generation of emulsions in millimeter.

Many organic or inorganic particles sized from nano to micronmeter are chosen as stabilizer, such as block copolymer micelles, latex and silica. Stabilizing particle should fulfil the partial wetting condition for water and oil. This is often achieved by surface modification of the solid particles making them more hydrophobic. The commonly used methods of surface modification include: chemical grafting(e.g. organosilanes on silica particles) [55], adsorption of surfactants prior to emulsification[56], adsorption of organic molecules and polymers [57], and adsorption of multivalent ions of opposite charge [58].

The emulsion type (oil-in-water (o/w), water-in-oil(w/o) or multiple) is controlled by the wettability of the solid particles[59], which is often characterized by the contact angle in water, θ_w. More hydrophilic particles favor o/w Pickering emulsions ($\theta_w < 90°$) while more hydrophobic particles favor w/o emulsions ($\theta_w > 90°$).
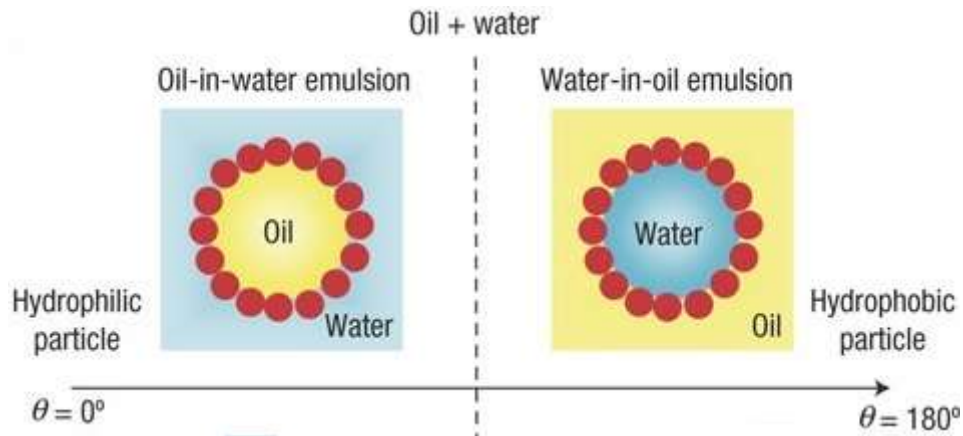
Figure 4. For oil–water mixtures , emulsion drops of oil in water or water in oil are stabilized with hydrophilic or hydrophobic particles respectively[60]. Adapted from Binks B. et al. (2006).

1.4 Fluid control in LOC device

Application of microfluidic products still face some challenges due to certain technical limitations, among which fluid manipulation often becomes a central source of complexity and mechanical failure. Fluids in microsystems are controlled via a number of external fields, namely pressure, electric, magnetic, acoustic, etc. The transport of liquid/gas or liquid/liquid interfaces in channels with partially wetting surfaces could be realized using capillary pressure gradients. The changes in surface tension gradient (Marangoni stresses[61]) could be adapted by thermal, chemical, electrical, or light gradients. According to Young-Laplace equation, $\Delta P=2\gamma H$, where ΔP is the pressure difference across the fluid interface, γ is the surface tension (or wall tension), H is the mean curvature, and R_1 and R_2 are the principal radii of curvature. The capillary pressure can be generated by adapting the wetting properties (surface tension γ) by one or more of the factors mentioned above, or geometry (mean curvature H). Thermal[62], magnetic[63] and electric[64] gradients have be utilized to drive droplets,

9

and modification of channel dimension successfully drive droplets in absence of a power supply[65]. In case of pressure-driven flow, the chemical gradient could also introduce changes in wettability and thus capable to move the air-water interface in a microchannel[66]. When it comes to manipulation of fluids in microsystems more versatile way, the driving forces and the surface characteristics are usually coupled.

1.5 Particle separation in microfluidic devices

Apart from microparticles, the sorting and separation of other micron-sized objects in a continuous flow arise in numerous applications, including food sterilization[67], mining[68] and biochemical analyses[69]. For example, unwanted microorganism can be removed with the help of separation techniques in food samples[67]. In theradiagnostic processes, the separation techniques can be utilized in sorting living cells VS dead cells, cancer cells VS normal cells and malaria-infected cells VS healthy cells[70]. Sorting and separation of droplets[71] are also necessary since droplets could function as microreactors or for encapsulation in drug delivery and manufacturing industry, which requires uniformity and consistent product quality.

Based on operating principles, the sorting methods could be categorized into passive, active or combined ones. Passive techniques utilize the interaction between particles, channel structure and fluids field, and external fields are not involved. On the other hand, active techniques require external fields (e.g. electric[72], acoustic[73], gravity[2, 74, 75], etc.) but increase the particle sorting efficiency compared to passive techniques. Thus, passive separation techniques are chosen in applications where external energy is not

eligible to introduce, while active separation techniques can be used where higher particle sorting efficiency is the primary concern. In real-world applications, the passive techniques are sometimes coupled with external fields in order to enhance the separation and sorting performance. Among current separation strategies for particulate systems in microfluidic devices, deterministic lateral displacement (DLD) and pinched flow fractionation (PFF) are promising, as they can operate continuously and at high flow rates.

1.5.1 Deterministic lateral displacement (DLD)

Deterministic lateral displacement (DLD) utilizes arrays of cylindrical obstacles placed in the microchannel. Based on their size, the species are locked into periodic trajectories that exhibit lateral displacement as they pass through the gap between obstacles[1, 9, 71, 74, 76-81]. D is the diameter of the obstacle. The center-to-center distance between the adjacent obstacles is λ, and each row is shifted vertically by ελ relative to the previous row(shown in Fig. 5). The irreversible collisions between the particle and the obstacle introduces a lateral displacement and breaks the symmetry of the particle trajectory. When particles passing through the gap between obstacles, the asymmetric bifurcation of laminar flow around obstacles make the particles select their path deterministically base on their size. While smaller particle exhibits a "zigzag" shape trajectory, larger particle go straight through the gap between adjacent rows. In this way, different sizes of particles could be separated continuously[82], as shown Fig. 5. Apart from being employed as a flow-driven, passive separation method, DLD could also be

combined with external forces (f-DLD), to drive and separate particles. Gravity and electric fields have successfully drive the separation of suspended particles in force-driven DLD systems.
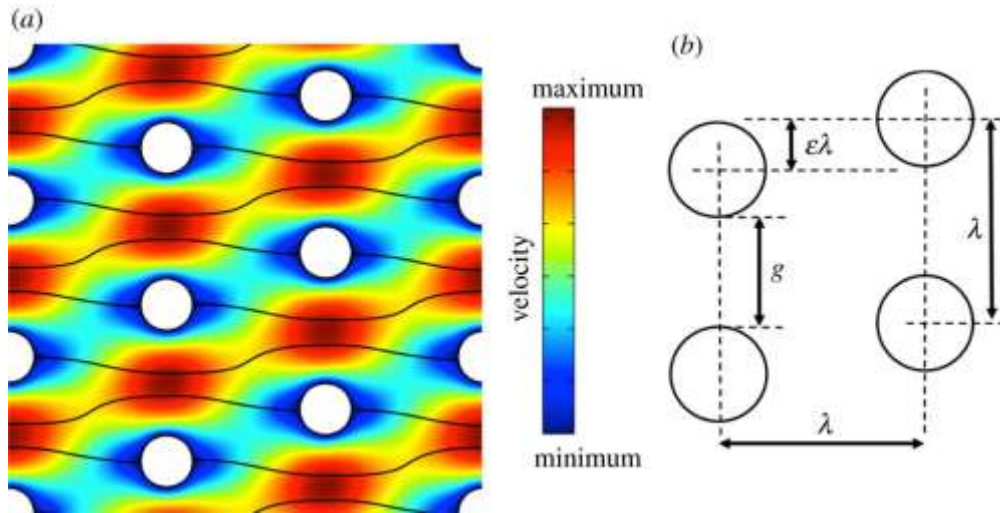
Figure 5. *Schematic illustration of the fluid streamlines (Re<<1) through an array of cylindrical obstacles. Each row is shifted vertically by ελ relative to the previous row, where λ is the inter-obstacle distance, ε is the row shift fraction and g the gap between the obstacles[82]. Adapted from Holmes, D et al. (2006).*

1.5.2 Pinched flow fractionation (PFF)

In pinched flow fractionation PFF, separation is performed as the species in the mixture are displaced laterally when they go through a constriction (pinched segment) first and then enter an expansion[2, 8, 83-87]. The PFF technique assumes that the fluid is incompressible, and no-slip condition, low Reynolds number and steady-state conditions are satisfied. In addition, it is based on the assumption that the particles do not perturb the fluid flow or interact with the channel walls. In laminar flow, particles have the tendency to follow the streamline passing through their centers. The mixture

of fluid and particles coming out of the pinched segment is separated by the spreading streamlines passing through them based on their sizes.

As shown in Fig. 6, buffer stream and particle solution are injected into the microchannel from separate inlets. By controlling the flow rates of both fluids, particles are forced on one of the sidewalls when they pass the pinched segment. Next, a force toward the center of the microchannel is exerted mainly on the larger particles, whereas a force toward the sidewall is exerted mainly on the smaller particles (Fig. 6b). Consequently, the slight difference of the particle displacements in the pinched segment is largely amplified in the expansion segment. Thus the particles could be separated according to their sizes in vertical direction as to channel wall.
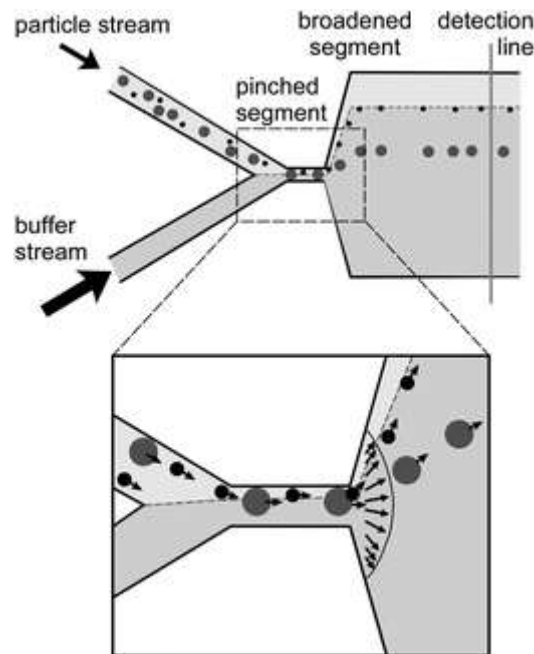
Figure 6. *Principle of pinched flow fractionation[8]. (a) In the pinched segment, particles are aligned to one sidewall; (b) particles are separated according to their sizes when they pass a constriction (pinched segment) first and then entering an expansion. Adapted from Yamada, M D et al. (2004).*

1.6 Highlight in our work

We developed a simple but versatile microfluidic platform employing semi-circular cylinder solid (PDMS) and fluid (bubble) obstacle in PDMS microchannel, to mimic the colloidal transport on solid-water (SWI) and air-water (AWI) in subsurface. Initially, we employ pressure-driven flow to pulse the particles in channel. While particles move downstream to the bubble or PDMS solid obstacle, they never stick on either AWI or SWI, but rather move around the obstacle and follow the streamline, exhibiting symmetric trajectories as to obstacle center. Later on, instead of pressure driven flow, gravity is employed to drive the particles through the channel and pass the obstacle. Here we observe both symmetric and asymmetric particle trajectories as to obstacle center.

The flows involved in microfluidics are typically Stokes flows, in that, the corresponding Reynolds numbers are negligible (Re $\ll$ 1). Here we use collision model[1] to describe the trajectories of particles passing an obstacle. The particle trajectory is characterized by an offset, which is defined as its distance from the line passing through the obstacle center along the direction of motion far away from the obstacle. The interaction between a particle and an obstacle determines its subsequent trajectory, since the interaction is subject to size, shape, density or some other properties of particles. In this model there are two types of particle–obstacle collisions. The hydrodynamic collisions are reversible in the absence of inertia and thus there is no net lateral displacement (symmetric trajectories). The touching collisions are irreversible,

since hard-core repulsion prevents the particle from getting closer than minimum separation to the obstacle, which gives rise to a net lateral displacement (asymmetric trajectories).

We analyze the motion and interactions of a suspended spherical particle passing through a constriction between a fixed half-circular cylindrical obstacle and a plane wall, to better understand the mechanisms of microfluidic separation techniques. We use the critical parameter to understand the behavior of particle trajectories passing through a constriction. We observe that the critical parameter increases with increasing particle radius, which is the underlying mechanism for the microfluidic separation technique called pinched flow fractionation[86]. For a given size of constriction, the larger the particle size the more it 'feels' the effect of the constriction, resulting in a larger critical parameter in the presence of the non-hydrodynamic interactions. The key finding of this work that the critical parameter observed (in microfluidic experiment and COMSOL simulation) to increase with particle size. Therefore, size-based particle separation is possible.

Chapter 2.   Material and Method

2.1 Materials

Elastomer (Dow Corning Sylgard 184) is purchased from Robert McKeown Inc. (Branchburg, NJ). Sillicon wafer is purchased from University Wafer (Boston, MA). SU-8 2025 and SU-8 2075 photoresist and developer are purchased from Microchem Corp. (Newton, MA). Coverslips（12-545-J 22×60–1）purchased from Thermo Fisher Scientific Inc. (Pittsburg, PA). Sodium Dodecyl Sulfate (SDS) is purchased from Sigma-Aldrich (St. Louis, MO) and diluted with deionized water to a final concentration of 5mM. Silica particles (diameter = 10, 15, 20µm) are purchased from Bang's Laboratories (Fishers, IN) and sulfate polystyrene latex particles (diameter = 3, 5, 9, 20µm) are purchased from Thermo Fisher Scientific Inc. (Pittsburg, PA). Unless mentioned otherwise, all chemicals are used as received.

2.2 Fabrication

Molds for the PDMS channels are fabricated using conventional photolithography[11] method. Micropatterns, which serve as template for the microfluidic channels, are fabricated on a silicon wafer to reach a final thickness of either 33µm (SU-8 2025) or 100µm (SU-8 2075). The elastomer base and curing agent are mixed in a 10:1 ratio and then spin-coated onto the mold, followed by degassing under vacuum for 20 min. Following degassing, the elastomer is cured overnight at 70 °C, then is peeled off from the mold. The Fluid ports are punched into the PDMS using a 0.75 mm Uni-core biopsy

punch (Harris, Ted Pella, Inc. USA). The microchannel and coverslip are then exposed to oxygen plasma (Technics PEII A/B) and immediately aligned and sealed.

Two different microfluidic devices are fabricated. First a standard T-channel[88] is employed to study the particle trajectories around a captive bubble (see Fig. 7A). Second a channel with a cylindrical obstacle is fabricated to study the particle trajectories around a solid obstacle (see Fig. 7B). All the channels have a rectangular cross-sections. Dimensions of channels are shown in Table 2.

2.3 Characterization

The final dimensions of the microchannels were measured by the Optical Profilometer function of a 3D laser scanning microscope (Keyence VK–X100) and processed by VK Viewer software.
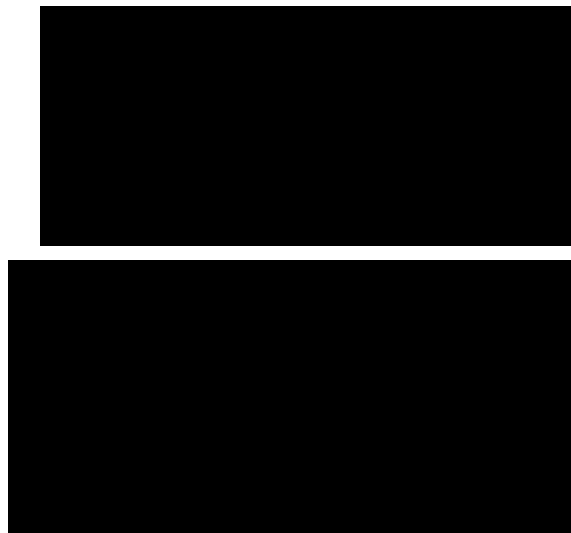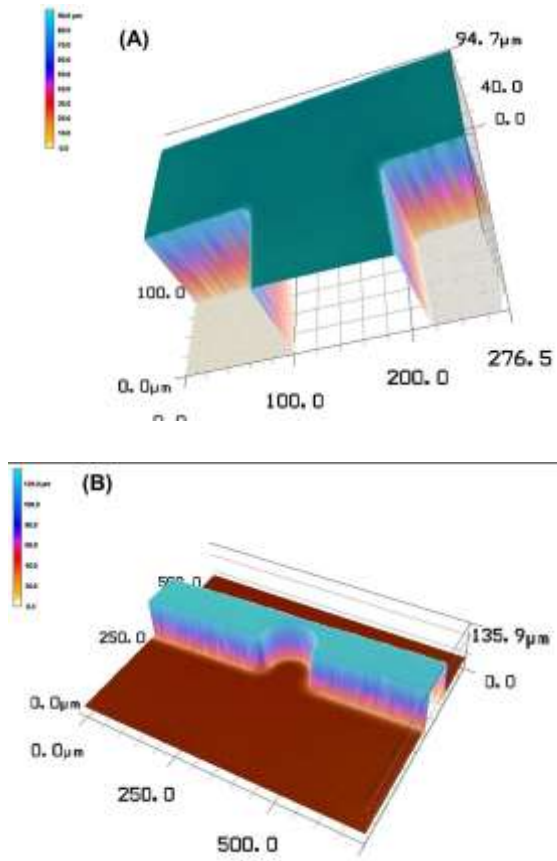
Figure 7. 3D optical Microscopic image of (A) T–channel and (B) a channel with a solid obstacle. Schematic illustration of (C) T–channel and (D) a channel with a solid obstacle. Dimensions of channels are shown in Table 1

No.	Width W_1 (μm)	Width W_2 (μm)	Height H (μm)	Obstacle Radius R (μm)	Gap G (μm)
1	100	100	33	-	-
2	50	50	33	-	-
3	100	100	100	-	-
4	100	-	100	60	20
5	100	-	100	60	30
6	100	-	100	60	40

Table 2. Characteristic dimensions of the T-shape and solid obstacle channel studied in this work. As shown in Fig.1 (A) and (B), the width W_1 of the channel that carries liquid phase, the width W_2 of the channel that carries liquid phase (only T-shaped channel), the radius R of the solid obstacle (only solid obstacle channel), the gap G between the obstacle & the bottom of channel (only solid obstacle channel) and the height H of the channel.

Sulfate polystyrene(PS) latex particles are dispersed in a 5mM aqueous sodium dodecyl sulfate (SDS) solutions to a final concentration of approximately 0.4% (w/v) while silica particles are dispersed in deionized water to a final concentration of approximately 0.2% (w/v), followed by sonication for two minutes before each experiment. We flow PS particle solution in the horizontal channel and pump air downwards in the vertical channel so as to create a bubble right at the T junction. By adjusting the pressure difference from all three inlets, we are able to change the bubble size and flow rate. Images are captured by Nikon Confocal microscope and are processed by NIS Elements Viewer software. The air bubble and the flow of the polystyrene particle solution are controlled by a pressure system. Through plastic tubing and steel needles at the end, fluids could be infused via ports at the end of

channels. Pressure difference between the inlet and outlet of the T-channel is 0.1-0.3psi, giving a flow rate of approximately 200µm/s. Silica particle solution is injected into channel using a Hamilton Syringe to pump in air column. The device is leveled on the microscope. The silica particles were driven by gravity when tilting the entire microscope at about 15° to 20°. The Images were captured using MC352+ microscope and were processed by Motic image software.

Chapter 3.   Result and Discussion

3.1 Determination of critical impact parameter

We employ a simple model[1] to describe the trajectories of particles past an obstacle. In this model there are two types of particle–obstacle collisions that are characterized by the incoming offset, b_{in}, defined as the vertical distance between the asymptotic line of particle trajectory and the obstacle center before the collision (illustrated in Fig. 8). Correspondingly, we define the outgoing offset, b_{out}, as the vertical distance between the asymptotic line of particle trajectory and the obstacle center after the collision. If the incoming offset is larger than a critical value defined as b_c, the particle trajectory is symmetrical passing across the obstacle, as predicted from Stokes flow (see the top trajectory in Fig. 8), i.e. $b_{in} = b_{out}$. In this paper we refer to this type of collision as reversible. The second type of collision, referred to as irreversible collision, occurs when the incoming offset, b_{in} is below or equal to some critical value, b_c (bottom two trajectories in Fig. 8), leads to outgoing offsets that no longer depend on the impact parameter and that are always equal to b_c.
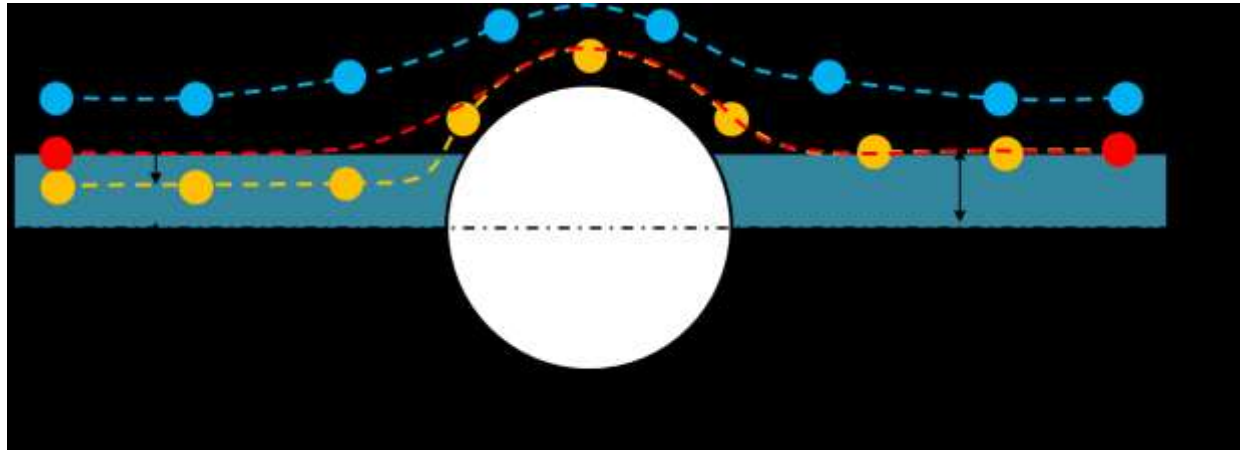
Figure 8. *Schematic illustration of reversible and irreversible particle trajectories around a fixed sphere obstacle in particle–obstacle collision model. The symmetric trajectory on top shows reversible, purely hydrodynamic collisions where $\boldsymbol{b_{in}} > \boldsymbol{b_c}$ and $\boldsymbol{b_{in}} = \boldsymbol{b_{out}}$. The asymmetric trajectory on bottom shows irreversible, touching collisions where $\boldsymbol{b_{in}} < \boldsymbol{b_c}$ and $\boldsymbol{b_{out}} = \boldsymbol{b_c}$.*

3.2 Particle trajectories under pressure-driven flow

Solutions with dispersed polystyrene particles were injected in the horizontal channel of a T-shaped microfluidic device. The trajectories of the particles were monitored as they flew past the solid or bubble obstacle under pressure-driven flow. We monitor both the incoming and outgoing offsets. We find that under pressure-driven flow the particle trajectories are always symmetrical for both solid and fluid obstacles. As shown in Fig.9, all data points fall on the asymptotic line "$b_{in} = b_{out}$" (slope=1). The only exception we observe is in the case of the fluid obstacle when the diameter of the particle is comparable to the minimum gap at the constriction. Under this configuration we observe, in some instances, that b_{out} is less than b_{in} because the particles go above or below the center point (where the radius of the bubble is largest) to go around the obstacle. The meniscus is unlikely to be perfectly cylindrical, due in part to pinning of the contact line on the upper and lower surfaces of the microfluidic device. This

distortion in the shape of the meniscus allows for the particle to move on the z-direction as they navigate a highly pinched constriction. In all other instances the trajectories are symmetrical and the particles travel in 2D.
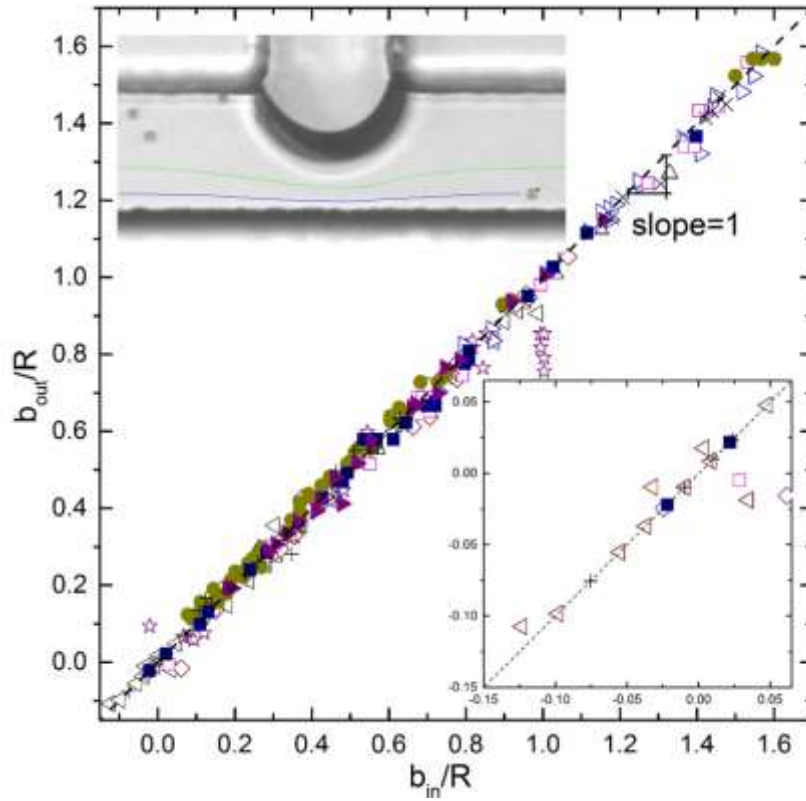
Figure 9. Outgoing offset (b_{out}) as a function of the incoming offset (b_{in}), both normalized with the obstacle radius (R) for polystyrene particles in pressure-driven flow. Here all solid symbols indicate trajectories for solid obstacle while hollow symbols indicate trajectories for fluid obstacle. The inset illustrates the incoming and outgoing offsets of particles which interact the non-cylindrical part of obstacles. The dash line illustrate the trend line "bin=bout". The gaps (G in μm), channel height(H) and particle radius (a in μm) in the figure are (△), H=100, G=4.4, a=1.5; (▽), H=100, G=31.2, a=1.5; (◁) , H=100 , G=13, a=2.5; (▷), H=100, G=13, a=2.5; (◇), H=100, G=30,a=4.5; (□) ,H=100, G=10,a=4.5; (☆), H=100, G=6,a=10; (●), H=100, G=40,a=4.5; (■), H=100, G=30,a=4.5; (▶), H=100, G=20,a=4.5; (+), H=33 G=47, a=1.5; (×), H=33, G=113, a=2.5

In contrast, the presence of critical offset b_c has been commonly observed in previous pressure driven DLD systems[78, 80, 86]. It has also been theoretically predicted

that in a flow driven environment the irreversible collision exists in a particle-obstacle (solid) interaction. Specifically, in a pressure driven environment when the particle comes to a particle-obstacle collision with an incoming offset that is smaller than its critical offset b_c, it will move in a asymmetric trajectory.

One possible explanation for the difference between our experimental results and what has been observed in previous related work might be that due to the restriction of the top wall, the incoming offset for every particle inside the channel is always larger than its critical offset and particles cannot get closer to obstacle. In particular, in most of our experiments, we observed that the center of the obstacle tends to align with the top wall nicely, which limits the incoming offset for certain size of particles to be always higher than the particle radius. In this case, if the critical offset for a certain size of particles is smaller than the radius of the particle, then $b_{in} > b_c$ holds true, and the particles will only move in symmetric trajectories as a result.

To test our explanation, we normalize the outgoing offset (b_{out}) and particle radius (a) both with the obstacle radius (R) for each particle and the normalized outgoing offset is plotted as a function of the normalized particle radius in Figure 10. We should recognize the case when a bubble is big enough (central angle is more than 180°) that it has a ridge of major arc, where negative bin and bout could be observed. As mentioned above, the meniscus of bubble is unlikely to be perfectly cylindrical, especially the part on top and bottom. Consequently the particles interact with those part could not be characterized by the "particle-obstacle" model (inset in Fig. 9). As a

result, those data are cleared up and not shown in Fig. 10. We observed that all symbols

(only particles interacting with cylindrical part of obstacle) fall above the asymptotic

line representing $b_{out} = a$, i.e. b_{out} is always larger than the particle radius, which

supports our explanation.
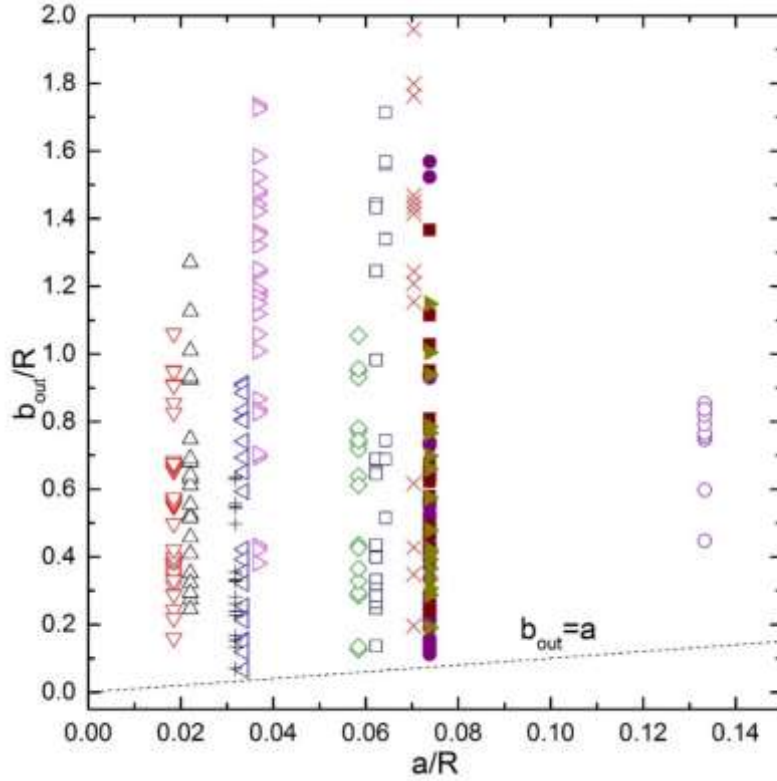
Figure 10. *Outgoing offset (b_{out}) as a function of the particle radius (a), both normalized with the obstacle radius (R) for polystyrene particles in pressure-driven flow. The obstacle type and particle radius (a in μm) in the figure are: ($\triangle$), H=100, G=4.4, a=1.5; ($\triangledown$), H=100, G=31.2, a=1.5; ($\triangleleft$), H=100, G=13, a=2.5; ($\triangleright$), H=100, G=13, a=2.5; ($\diamond$), H=100, G=30,a=4.5; ($\square$) ,H=100,G=10,a=4.5; ($\circ$), H=100, G=6,a=10; ($\bullet$) H=100, G=40,a=4.5; ($\blacksquare$), H=100, G=30,a=4.5; ($\blacktriangleright$) H=100, G=20,a=4.5; (+), H=33, G=47, a=1.5; ($\times$), H=33, G=113, a=2.5.*

3.3 Force driven particle trajectories

The trajectories of silica particles driven by gravity is characterized as the particles move past either a solid or fluid obstacle. For a given particle size and obstacle radius, we measure incoming offset (b_{in}) and outgoing offset (b_{out}) of each trajectory. In contrast to pressure-driven flow, the result is similar to the macroscopic gravity driven pinched-flow–fraction (PFF) study[86] where asymmetric trajectories and size-based separation are observed due to hard-core particle- obstacle repulsion.

We observe both hydrodynamic (blue symmetric trajectories in Fig. 8) and touching collisions (yellow asymmetric trajectories in Fig. 8) for both solid and fluid obstacles. The critical offset (b_c) is derived by averaging all b_{out} smaller than the transitioning point where "$b_{in} = b_{out}$" (horizontal dash line in Fig. 11). The data points in plateau area describe irreversible collisions, which occur when $b_{in} < b_c$. All trajectories with $b_{in} < b_c$ are asymmetric. The data points on the asymptotic line "$b_{in} = b_{out}$" (slope=1) describe reversible collisions, which occur when $b_{in} \geq b_c$. We also observe that the critical offset (b_c) for a given particle size around a solid obstacle is always larger than the one observed for the trajectories around of bubble (hollow symbols are all below the solid symbols in Fig. 11), for a given obstacle radius(R), particle radius (a) and gap (G). It is more straightforward in Fig. 12, particles will continue their paths on the bubble a little bit after they pass the bottom point (A); while particles will leave the solid obstacle almost right after they pass the bottom point (B).
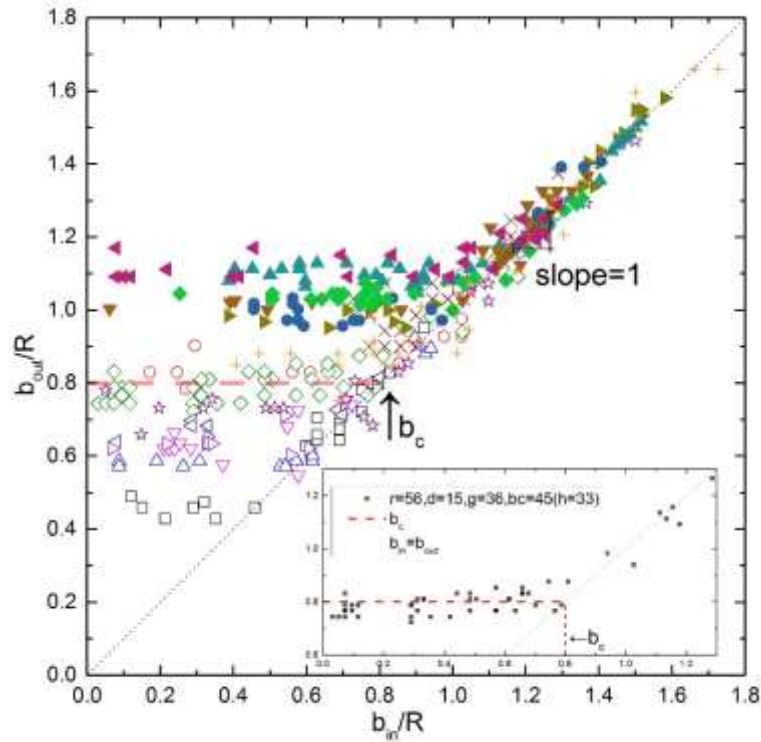
Figure 11. *Scaling of outgoing offset (b_{out}) and incoming offset (b_{in}) with the obstacle radius(R) for silica particles with various radius (a) driven by gravity force. Solid symbols indicate solid obstacle while hollow symbols indicate fluid obstacle. The inset shows an example on how bc is clarified. The gaps (G in µm) and particle radius (a in µm) in the figure are: (□), R=65, a=5, G=34, b_c=34; (○), R=54, a=5, G=40, b_c=41; (△), R=68, a=7.5, G=36, b_c=46; (▽),R=68, a=7.5, G=32, b_c=50; (◇), R=56, a=7.5, G=36, b_c=45; (◁), R=68, a=10, G=36, b_c=53; (▷), R=65, a=10, G=38, b_c=48; (☆), R=54, a=10, G=47, b_c=47; (×), R=33, a=10, G=24, b_c=32; (+), R=33, a=5, G=24, b_c=29; (▼), R=63, a=5, G=27, b_c=61; (●), R=64, a=7.5, G=38,b_c=63; (▲), R=62, a=10, G=38, b_c=68; (▶), R=62, a=5, G=38, b_c=61; (◆), R=62, a=7.5, G=25, b_c=65; (◀), R=63, a=10, G=27, b_c=69.*

Since a critical offset (b_c) is observed for all particles around obstacles in channel, we also observe the size-based separation of microfluidic system. When we flow the mixture of different sizes of particle in the channel, the particles flow around the same obstacle (same radius(R) and gap (G)). In this case, larger particles show larger outgoing offset (b_{out}) and consequently larger critical offsets (b_c) (see different particles' b_c in caption of Fig. 11 and trajectories of 10µm and 20 µm silica particles

in Fig.12). When particles have touching collisions with obstacle, the center of a larger particle is more distant from the obstacle center than smaller ones, thus the outgoing offset (b_{out}) is larger.
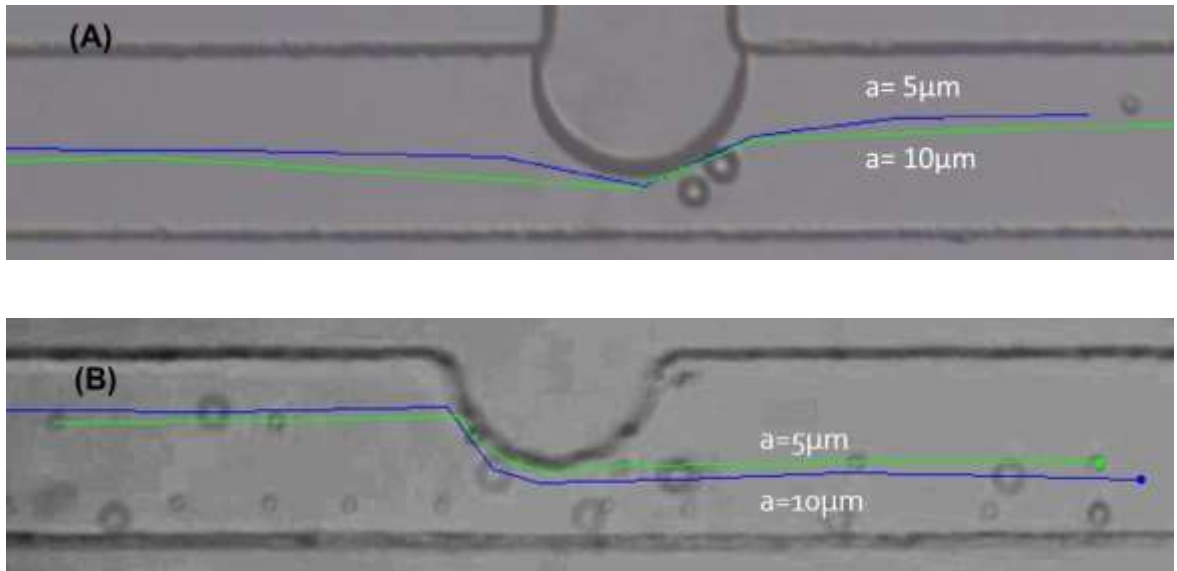
Figure 12. Separation of 10 and 20 µm silica particles around fluid (A) and solid (B) obstacle.

To further investigate the size-based separation behavior of particles in the microfluidic system, we show the non-dimensional critical offset as a function of non-dimensional particle radius in Fig. 13. When different sizes of particle pass the same obstacle, b_c nearly linearly increases with a, which coincides with previous macroscopic studies[78, 80]. Similar to Fig. 11, the critical offset (b_c) of certain size of particles around solid obstacle is larger than the one observed for the trajectories around of bubble (hollow symbols are all below the solid symbols) in small a/R regime.

Due to the error occurred in microfabrication, the PDMS solid obstacle is less smooth than the fluid bubble. Experiment and modeling show that surface roughness could

reduce the pull-off force between particle and obstacle[89, 90], which could balance the hydrodynamic restraining torque acting on the particles to obstacle surface. As a result, more net pull-off force is required when same silica particle leaves the smooth bubble surface than the rougher PDMS surface. This larger restrain causes the extension of particle trajectory on surface, which leads to smaller outgoing offset (b_{out}) and critical offset (b_c). However, the hollow symbols have more scatter than solid symbols, which could result from the deformation of bubble due to any vibration in experiment (e.g. when tilt the microscope), air tightness of microfluidic system and particle interaction with bubble. Improvement could be made on decrease the surface roughness of microchannel in design and fabrication step, as well as the robustness of setup in experimental step.
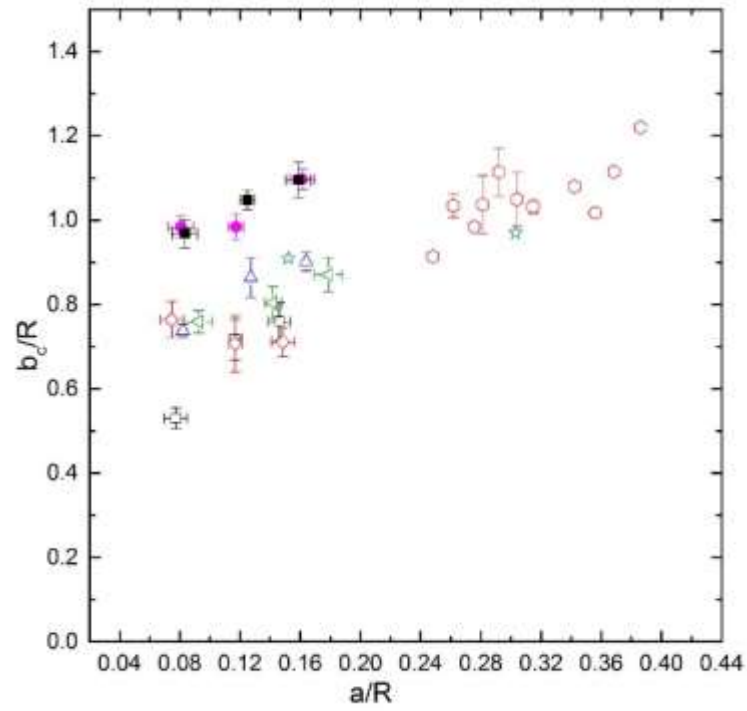
Figure 13. *Scaling of critical offset (**b**c) and particle radius (a) with the obstacle radius(R) for silica particles. The gaps (G in μm) and particle radius (a in μm) in the figure are: (□), g=35, R=68;(○), g=25, R=68; (Δ), g=27, R=61; (◇) g=50, R=68; (◁),g=40, R=55; (☆) g=25, R=33; (●), g=38, R=62; (■) g=27, R=62.*

Chapter 4. Conclusion

We developed a microfluidic-based platform with semi-circular cylinder solid (PDMS) or fluid (bubble) obstacle in PDMS microchannel, to real-time monitor the colloidal transport on solid-water (SWI) and air-water (AWI) within small Reynolds numbers regime (Re $\ll$1). The particle-obstacle interaction is simplified as a suspended spherical particle passing through a constriction between a fixed half-circular cylindrical obstacle and a plane wall.

 The particle trajectory is described by an offset, which is defined as its distance from the line passing through the obstacle center along the direction of motion far away from the obstacle. We use the critical offset (b_c) to understand the behavior of particle trajectories passing through a constriction. While incoming offset $b_{in} < b_c$, touching collisions occur with asymmetric trajectories. When $b_{in} \geq b_c$, hydrodynamic collisions occur with symmetric trajectories.

 We manage to impulse particles downstream towards the obstacles via two method: pressure driven flow or gravity force. While under pressure-driven flow, particles never get adsorbed on either AWI or SWI, but rather move around the obstacle and follow the streamline, exhibiting symmetric trajectories as to obstacle center and no critical offset (b_c) is clarified. In contrast, under gravity force, we observe both symmetric and asymmetric particle trajectories as to obstacle center. We observe that the critical offset increases with increasing particle radius in the presence of the non-hydrodynamic interactions, which coincides with the previous macroscopic studies[78, 80].Given similar

obstacle radius(R), particle radius (a) and gap (G), the critical offset (b_c) of particles

around solid obstacle is bigger than that of bubble. The key finding of this work is the

critical parameter observed in microfluidic experiment increase with particle size and

confirmed by COMSOL simulation. Therefore, size-based particle separation around

single obstacle is possible.

Reference

1. Balvin, M., et al., *Directional Locking and the Role of Irreversible Interactions in Deterministic Hydrodynamics Separations in Microfluidic Devices.* Physical Review Letters, 2009. **103**(7): p. 078301.

2. Risbud, S.R. and G. Drazer, *Mechanism governing separation in microfluidic pinched flow fractionation devices.* Microfluidics and Nanofluidics, 2014. **17**(6): p. 1003-1009.

3. Huang, F.C., C.S. Liao, and G.B. Lee, *An integrated microfluidic chip for DNA/RNA amplification, electrophoresis separation and on‐line optical detection.* Electrophoresis, 2006. **27**(16): p. 3297-3305.

4. Gagnon, Z.R., *Cellular dielectrophoresis: applications to the characterization, manipulation, separation and patterning of cells.* Electrophoresis, 2011. **32**(18): p. 2466-2487.

5. Marle, L. and G.M. Greenway, *Microfluidic devices for environmental monitoring.* TrAC Trends in Analytical Chemistry, 2005. **24**(9): p. 795-802.

6. Potiguar, F.Q., G.A. Farias, and W.P. Ferreira, *Self-propelled particle transport in regular arrays of rigid asymmetric obstacles.* Physical Review E, 2014. **90**(1): p. 012307.

7. Yohan, D., et al., *Size-Dependent Gold Nanoparticle Interaction at Nano--Micro Interface Using Both Monolayer and Multilayer (Tissue-Like) Cell Models.* Nano-Micro Letters, 2016. **8**(1): p. 44-53.

8. Yamada, M., M. Nakashima, and M. Seki, *Pinched Flow Fractionation: Continuous Size Separation of Particles Utilizing a Laminar Flow Profile in a Pinched Microchannel.* Analytical Chemistry, 2004. **76**(18): p. 5465-5471.

9. Huang, L.R., et al., *Continuous particle separation through deterministic lateral displacement.* Science, 2004. **304**(5673): p. 987-990.

10. Whitesides, G.M., *The origins and the future of microfluidics.* Nature, 2006. **442**(7101): p. 368-373.

11. Zhou, J., A.V. Ellis, and N.H. Voelcker, *Recent developments in PDMS surface modification for microfluidic devices.* Electrophoresis, 2010. **31**(1): p. 2-16.

12. Zhang, W., et al., *PMMA/PDMS valves and pumps for disposable microfluidics.* Lab on a Chip, 2009. **9**(21): p. 3088-3094.

13. Vourdas, N., et al., *Plasma processing for polymeric microfluidics fabrication and surface modification: effect of super-hydrophobic walls on electroosmotic flow.* Microelectronic Engineering, 2008. **85**(5): p. 1124-1127.

14. Ogończyk, D., et al., *Bonding of microfluidic devices fabricated in polycarbonate.* Lab on a Chip, 2010. **10**(10): p. 1324-1327.

15. Thomson, D.A., J.P. Hayes, and H. Thissen. *Protein patterning in polycarbonate microfluidic channels.* in *Microelectronics, MEMS, and Nanotechnology.* 2004. International Society for Optics and Photonics.

16. Metz, S., R. Holzer, and P. Renaud, *Polyimide-based microfluidic devices.* Lab on a Chip, 2001. **1**(1): p. 29-34.

17. Metz, S., et al., *Polyimide microfluidic devices with integrated nanoporous filtration areas manufactured by micromachining and ion track technology.* Journal of Micromechanics and Microengineering, 2003. **14**(3): p. 324.

18. Liu, A.-L., et al., *Plastified poly(ethylene terephthalate) (PET)-toner microfluidic chip by direct-printing integrated with electrochemical detection for pharmaceutical analysis.* Talanta, 2006. **68**(4): p. 1303-1308.

19. Lee, N.Y., *Recent Progress in Lab-on-a-Chip Technology and Its Potential Application to Clinical Diagnoses.* Int Neurourol J, 2013. **17**(1): p. 2-10.

20. Tang, L. and N.Y. Lee, *A facile route for irreversible bonding of plastic-PDMS hybrid microdevices at room temperature.* Lab on a Chip, 2010. **10**(10): p. 1274-1280.

21. Kim, S.-K., *Springer handbook of marine biotechnology.* 2015: Springer.

22. Costantini, F., et al. *Microfluidic chips with integrated amorphous silicon sensors for point-of-care testing.* in *Chemical and Biological Microsystems Society.* 2014.

23. Ghallab, Y.H. and W. Badawy, *Lab-on-a-chip: techniques, circuits, and biomedical applications.* 2010: Artech House.

24. Chang, L.-C., et al., *Experimental study on imbibition displacement mechanisms of two-phase fluid using micro model.* Environmental Earth Sciences, 2009. **59**(4): p. 901-911.

25. Wu, M., et al., *Single- and two-phase flow in microfluidic porous media analogs based on Voronoi tessellation.* Lab on a Chip, 2012. **12**(2): p. 253-261.

26. Dawe, R.A., A. Caruana, and C.A. Grattoni, *Microscale Visual Study of End Effects at Permeability Discontinuities.* Transport in Porous Media, 2011. **86**(2): p. 601-616.

27. Lazouskaya, V., Y. Jin, and D. Or, *Interfacial interactions and colloid retention under steady flows in a capillary channel.* Journal of Colloid and Interface Science, 2006. **303**(1): p. 171-184.

28. Berejnov, V., N. Djilali, and D. Sinton, *Lab-on-chip methodologies for the study of transport in porous media: Energy applications.* Lab on a Chip - Miniaturisation for Chemistry and Biology, 2008. **8**(5): p. 689-693.

29. Kumar Gunda, N.S., et al., *Reservoir-on-a-Chip (ROC): A new paradigm in reservoir engineering.* Lab on a Chip, 2011. **11**(22): p. 3785-3792.

30. Wan, J. and J.L. Wilson, *Colloid transport in unsaturated porous media.* Water Resources Research, 1994. **30**(4): p. 857-864.

31. Wan, J. and J.L. Wilson, *Visualization of the role of the gas-water interface on the fate and transport of colloids in porous media.* Water Resources Research, 1994. **30**(1): p. 11-23.

32. Lanning, L.M. and R.M. Ford, *Glass micromodel study of bacterial dispersion in spatially periodic porous networks.* Biotechnology and Bioengineering, 2002. **78**(5): p. 556-566.

33. Karadimitriou, N.K., et al., *A novel deep reactive ion etched (DRIE) glass micro-model for two-phase flow experiments.* Lab on a Chip, 2012. **12**(18): p. 3413-3418.

34. Baumann, T. and C.J. Werth, *Visualization and Modeling of Polystyrol Colloid Transport in a Silicon Micromodel.* Vadose Zone Journal, 2004. **3**(2): p. 434-443.

35. Prasad, V., D. Semwogerere, and R.W. Eric, *Confocal microscopy of colloids.* Journal of Physics: Condensed Matter, 2007. **19**(11): p. 113102.

36.   Sharma, P., *Geological disposal of nuclear waste: fate and transport of radioactive materials*. 2012: INTECH Open Access Publisher.

37.   Martin, C., et al., *Review of the effect of grinding media on flotation of sulphide minerals.* Minerals Engineering, 1991. **4**(2): p. 121-132.

38.   Rubio, J., M. Souza, and R. Smith, *Overview of flotation as a wastewater treatment technique.* Minerals engineering, 2002. **15**(3): p. 139-155.

39.   Zhao, Y., Y. Deng, and J. Zhu, *Roles of surfactants in flotation deinking.* Progress in Paper Recycling, 2004. **14**(1): p. 41-45.

40.   Albijanic, B., et al., *A relationship between the bubble–particle attachment time and the mineralogy of a copper–sulphide ore.* Minerals Engineering, 2011. **24**(12): p. 1335-1339.

41.   Verrelli, D.I., P.T. Koh, and A.V. Nguyen, *Particle–bubble interaction and attachment in flotation.* Chemical Engineering Science, 2011. **66**(23): p. 5910-5921.

42.   Nguyen, A.V., J. Nalaskowski, and J.D. Miller, *The dynamic nature of contact angles as measured by atomic force microscopy.* Journal of colloid and interface science, 2003. **262**(1): p. 303-306.

43.   Taran, E., et al., *Anomalous Time Effect on Particle− Bubble Interactions Studied by Atomic Force Microscopy.* Langmuir, 2009. **25**(5): p. 2797-2803.

44.   Ozdemir, O., et al., *Surface chemistry aspects of coal flotation in bore water.* International Journal of mineral processing, 2009. **92**(3): p. 177-183.

45.   Ozdemir, O., et al., *Contact angle and bubble attachment studies in the flotation of trona and other soluble carbonate salts.* Minerals Engineering, 2009. **22**(2): p. 168-175.

46.   Subasinghe, G.N. and B. Albijanic, *Influence of the propagation of three phase contact line on flotation recovery.* Minerals Engineering, 2014. **57**: p. 43-49.

47.   Fan, X., et al., *Attachment of solid particles to air bubbles in surfactant-free aqueous solutions.* Chemical engineering science, 2004. **59**(13): p. 2639-2645.

48.   Nguyen, A. and H.J. Schulze, *Colloidal science of flotation*. Vol. 118. 2003: CRC Press.

49.   Yoon, R.-H., *The role of hydrodynamic and surface forces in bubble–particle interaction.* International Journal of Mineral Processing, 2000. **58**(1): p. 129-143.

50.   Beneventi, D., O. Baudouin, and P. Nortier, *Semi-empirical modelling and management of flotation deinking banks by process simulation*. 2010: INTECH Open Access Publisher.

51.   Pickering, S.U., *CXCVI.-Emulsions.* Journal of the Chemical Society, Transactions, 1907. **91**(0): p. 2001-2021.

52.   Timgren, A., et al., *Starch particles for food based Pickering emulsions.* Procedia Food Science, 2011. **1**: p. 95-103.

53.   Frelichowska, J., et al., *Topical delivery of lipophilic drugs from o/w Pickering emulsions.* International journal of pharmaceutics, 2009. **371**(1): p. 56-63.

54.   Arditty, S., et al., *Materials based on solid-stabilized emulsions.* Journal of colloid and interface science, 2004. **275**(2): p. 659-664.

55.   Barthel, H., *Surface interactions of dimethylsiloxy group-modified fumed silica.* Colloids and Surfaces A: Physicochemical and Engineering Aspects, 1995. **101**(2): p. 217-226.

56. Drelich, A., et al., *Evolution of water-in-oil emulsions stabilized with solid particles: Influence of added emulsifier.* Colloids and Surfaces A: Physicochemical and Engineering Aspects, 2010. **365**(1): p. 171-177.

57. Akartuna, I., et al., *General Route for the Assembly of Functional Inorganic Capsules.* Langmuir, 2009. **25**(21): p. 12419-12424.

58. P. Binks, B. and S. O. Lumsdon, *Stability of oil-in-water emulsions stabilised by silica particles.* Physical Chemistry Chemical Physics, 1999. **1**(12): p. 3007-3016.

59. Binks, B. and S. Lumsdon, *Influence of particle wettability on the type and stability of surfactant-free emulsions.* Langmuir, 2000. **16**(23): p. 8622-8631.

60. Binks, B.P. and R. Murakami, *Phase inversion of particle-stabilized materials from foams to dry water.* Nat Mater, 2006. **5**(11): p. 865-869.

61. Hu, H. and R.G. Larson, *Analysis of the Effects of Marangoni Stresses on the Microflow in an Evaporating Sessile Droplet.* Langmuir, 2005. **21**(9): p. 3972-3980.

62. Sammarco, T.S. and M.A. Burns, *Thermocapillary pumping of discrete drops in microfabricated analysis devices.* Aiche Journal, 1999. **45**(2): p. 350-366.

63. Bau, H.H., J.H. Zhong, and M.Q. Yi, *A minute magneto hydro dynamic (MHD) mixer.* Sensors and Actuators B-Chemical, 2001. **79**(2-3): p. 207-215.

64. Gallardo, B.S., et al., *ELectrochemical principles for active control of liquids on submillimeter scales.* Science, 1999. **283**(5398): p. 57-60.

65. Juncker, D., et al., *Microfluidic Capillary Systems for The Autonomous Transport of Bio/Chemicals*, in *Micro Total Analysis Systems 2002: Proceedings of the µTAS 2002 Symposium, held in Nara, Japan, 3–7 November 2002 Volume 2*, Y. Baba, S. Shoji, and A. van den Berg, Editors. 2002, Springer Netherlands: Dordrecht. p. 952-954.

66. Zhao, B., J.S. Moore, and D.J. Beebe, *Surface-directed liquid flow inside microchannels.* Science, 2001. **291**(5506): p. 1023-1026.

67. Fukushima, H., et al., *Rapid separation and concentration of food-borne pathogens in food samples prior to quantification by viable-cell counting and real-time PCR.* Applied and Environmental Microbiology, 2007. **73**(1): p. 92-100.

68. Li, X.-b., et al., *Separation of oil from wastewater by column flotation.* Journal of China University of Mining and Technology, 2007. **17**(4): p. 546-577.

69. Reyes, D.R., et al., *Micro total analysis systems. 1. Introduction, theory, and technology.* Analytical chemistry, 2002. **74**(12): p. 2623-2636.

70. Alshareef, M., et al., *Separation of tumor cells with dielectrophoresis-based microfluidic chip.* Biomicrofluidics, 2013. **7**(1): p. 011803.

71. Bowman, T., J. Frechette, and G. Drazer, *Force driven separation of drops by deterministic lateral displacement.* Lab on a Chip, 2012. **12**(16): p. 2903-2908.

72. Beech, J.P., P. Jonsson, and J.O. Tegenfeldt, *Tipping the balance of deterministic lateral displacement devices using dielectrophoresis.* Lab on a Chip, 2009. **9**(18): p. 2698-2706.

73. Collins, D.J., T. Alan, and A. Neild, *Particle separation using virtual deterministic lateral displacement (vDLD).* Lab on a Chip, 2014. **14**(9): p. 1595-1603.

74. Devendra, R. and G. Drazer, *Gravity Driven Deterministic Lateral Displacement for Particle Separation in Microfluidic Devices.* Analytical Chemistry, 2012. **84**(24): p. 10621-10627.

75.   Huh, D., et al., *A Gravity-Driven Microfluidic Particle Sorting Device with Hydrodynamic Separation Amplification.* Analytical chemistry, 2007. **79**(4): p. 1369-1376.

76.   McGrath, J., M. Jimenez, and H. Bridle, *Deterministic lateral displacement for particle separation: a review.* Lab on a Chip, 2014. **14**(21): p. 4139-4158.

77.   Loutherback, K., et al., *Deterministic Microfluidic Ratchet.* Physical Review Letters, 2009. **102**(4): p. 045301.

78.   Du, S. and G. Drazer, *Deterministic separation of suspended particles in a reconfigurable obstacle array.* Journal of Micromechanics and Microengineering, 2015. **25**(11): p. 114002.

79.   Risbud, S.R. and G. Drazer, *Directional locking in deterministic lateral-displacement microfluidic separation systems.* Physical Review E, 2014. **90**(1): p. 012302.

80.   Bowman, T.J., G. Drazer, and J. Frechette, *Inertia and scaling in deterministic lateral displacement.* Biomicrofluidics, 2013. **7**(6): p. 064111.

81.   Devendra, R. and G. Drazer, *One-dimensional linear array of cylindrical posts for size-based deterministic separation of binary suspensions.* arXiv preprint arXiv:1404.1337, 2014.

82.   Holmes, D., et al., *Separation of blood cells with differing deformability using deterministic lateral displacement.* Interface Focus, 2014. **4**(6).

83.   Maenaka, H., et al., *Continuous and size-dependent sorting of emulsion droplets using hydrodynamics in pinched microchannels.* Langmuir, 2008. **24**(8): p. 4405-4410.

84.   Ashley, J.F., C.N. Bowman, and R.H. Davis, *Hydrodynamic separation of particles using pinched-flow fractionation.* AIChE Journal, 2013. **59**(9): p. 3444-3457.

85.   Lu, X. and X. Xuan, *Inertia-Enhanced Pinched Flow Fractionation.* Analytical Chemistry, 2015. **87**(8): p. 4560-4565.

86.   Luo, M., et al., *Irreversibility and pinching in deterministic particle separation.* Applied Physics Letters, 2011. **99**(6): p. 064102.

87.   Vig, A.L. and A. Kristensen, *Separation enhancement in pinched flow fractionation.* Applied Physics Letters, 2008. **93**(20): p. 203507.

88.   Garstecki, P., et al., *Formation of droplets and bubbles in a microfluidic T-junction—scaling and mechanism of break-up.* Lab on a Chip, 2006. **6**(3): p. 437-446.

89.   Das, S.K., R.S. Schechter, and M.M. Sharma, *The Role of Surface Roughness and Contact Deformation on the Hydrodynamic Detachment of Particles from Surfaces.* Journal of Colloid and Interface Science, 1994. **164**(1): p. 63-77.

90.   Cheng, W., P.F. Dunn, and R.M. Brach, *Surface roughness effects on microparticle adhesion.* The Journal of Adhesion, 2002. **78**(11): p. 929-965.

Curriculum Vitae

Tianyu Yan was born to Yunxiang Yan and Xiaobing Hu on August 29th, 1992, in Hefei, China. In 2010, she attended Southeast University, Nanjing, China, where she earned her bachelor degree in Biomedical Engineering in 2014.

Tianyu moved to Baltimore in August 2014 for graduate study in the department of Chemical and Biomolecular Engineering, Johns Hopkins University. She joined in the Dr. Frechette's lab in November, 2014.